Sensors and Materials, Vol. 36, No. 4 (2024) 1707–1730
MYU Tokyo

S & M 3628

Design of a Wave Electric Power Generation System with Maximum Output Power

Chen-Ming Zhang,[1] Shou-Hua Gong,[1] Jin-Xing Zhang,[2]
Yu-Ping Chen,[3] and Cheng-Fu Yang[4,5*]

[1]Mechanical Design, Manufacturing and Automation of the School of Mechanical and Electrical Engineering, Shaanxi University of Science and Technology, Xi'an 710021, China
[2]School of Electronic Information and Artificial Intelligence, Shaanxi University of Science and Technology, Xi'an 710021, China
[3]School of Chemistry and Chemical Engineering, Shaanxi University of Science and Technology, Xi'an 710021, China
[4]Department of Chemical and Materials Engineering, National University of Kaohsiung, Kaohsiung 811, Taiwan
[5]Department of Aeronautical Engineering, Chaoyang University of Technology,Taichung 413, Taiwan

(Received February 5, 2024; accepted April 3, 2024)

Keywords: wave, electric power generation system, buoy, motion equations, maximum output power

In this study, we addressed the problem of maximum output power in wave energy devices by analyzing the forces acting on the buoy and oscillators under the influence of ocean waves. The motion models for both floating devices and oscillators were developed, and algorithms were devised to determine the maximum output power of wave energy devices. When the buoy was only undergoing linear motion, a second-order ordinary differential equation could be established with displacement as the unknown variable. The main objective of this study was to maximize power, which was composed of the power generated by the damper, with the damping coefficient as the decision variable. Additionally, it was necessary to consider the following constraints in the motion equations: gravity, buoyancy, wave excitation force, added inertia force, wave damping force, static water restoring force, and the reactive forces from the damper and spring. By solving an unconstrained minimization problem related to the damping coefficient, the solution to achieve maximum power during linear motion could be found. When the rotation of the buoy was considered, we needed to modify the objective function to include the contribution of the rotational damper and introduce the rotational damping coefficient as a decision variable. Furthermore, we needed to add torque analysis as a constraint to account for the rotational motion of the buoy. Ultimately, the wave electric power generation system would provide the optimal power design solution that took into account both linear and rotational motions of the buoy.

1. Introduction

The issue of insufficient energy in the 21st century has propelled the development of various new energy sources, aiming to reduce the dependence on traditional fossil fuels and mitigate

*Corresponding author: e-mail: cfyang@nuk.edu.tw
https://doi.org/10.18494/SAM5019

ISSN 0914-4935
https://myukk.org/

environmental impacts. Presently, the actively pursued types of new energy include solar power, wind power, hydropower, bioenergy, and geothermal energy. Entering the 2020s, economic development has been accelerating at an unprecedented pace, accompanied by significant challenges in the realms of energy and the environment. The focus of nations worldwide has now shifted towards the renewable energy industry, recognizing its pivotal role in sustainable development. Wave electric power, a relatively new renewable energy technology, harnesses the kinetic energy of ocean waves to generate electricity. Its significance is evident in several aspects.[1–3]

(a) Renewability: Waves are a continuous natural resource and are considered to be an infinite source of renewable energy, unlike finite fossil fuels, which are subject to depletion.
(b) Low environmental impact: The development and operation of wave electric power are environmentally friendly, with no greenhouse gas emissions, resulting in minimal environmental impact.
(c) Stability: Ocean waves are relatively stable, providing wave electric power systems with a reliable capacity for electricity generation. This stability contrasts with other renewable energy sources, such as wind power, which can be more variable depending on weather conditions.
(d) High energy density: Waves possess a considerable energy density, enabling effective capture and conversion of wave energy, which results in the production of substantial amounts of electricity.

However, despite the manifold advantages of wave electric power, it faces persistent technical and economic challenges.[4] Ongoing research and development efforts are essential to optimize efficiency and reduce costs, thereby ensuring the sustained progress and competitiveness of this promising renewable energy technology. Wave energy, derived from the vast expanses of the oceans, holds tremendous potential for significantly contributing to the global energy mix. This study is specifically focused on optimizing a wave energy conversion system to maximize its power output. The research hones in on the power generation of a wave energy device, assuming the presence of a pre-existing wave energy conversion system. This system primarily comprises a floater and a pendulum.[5] Propelled by the motion of ocean waves, the floater's movement induces corresponding motion in the pendulum. The design proposed in this project primarily involves a buoy and a pendulum. As influenced by ocean waves, the buoy undergoes motion, subsequently driving the pendulum's movement.[6,7] The relative motion between these two components facilitates the operation of a damper to convert this motion into usable energy output. Azam *et al.* identified the optimal and suboptimal resonant buoys for power take-off (PTO) systems using external stiffness and damping parameters. In the optimal and suboptimal PTO modes for conventional waves, the energy conversion efficiency increased by 8.4% and 7.4%, respectively.[8]

Lai *et al.* studied the "Haiyuan 1" buoy, the heave motion mode of which was modified to a vertical swinging motion mode. The results indicated that the hydrodynamic performance of the vertical swinging buoy was effectively improved compared with that of the heaving buoy.[9] Ahmed *et al.* studied the influence of buoy geometry variations on PTO power performance, using cylindrical hemisphere (C-HS) and S-shaped buoys as examples. The PTO integrated into

the S-shaped buoy led to a 26% higher input power than the PTO integrated into the C-HS buoy.[10] Most current studies focus on capturing the single-degree-of-freedom kinetic energy of buoys. For multiple-degrees-of-freedom oscillating buoy wave energy conversion systems, the structure and extracted key components, including the buoy, pendulum, damper, and spring, were simplified for mechanical analysis. When the buoy undergoes linear motion only, with the objective function being the maximum power produced by the damper and the damping coefficient being the decision variable, the motion equation under the influence of gravity, buoyancy, wave excitation force, added inertia force, wave damping force, static water restoring force, and the reaction forces of the damper and spring was established as the constraint condition, forming an unconstrained minimization problem regarding the damping coefficient. We determined the maximum power under linear motion. Further incorporating buoy rotation, the optimal power design scheme was obtained by adding the contribution of the rotational damper to the objective function, increasing the number of decision variables for the rotational damping coefficient, and incorporating torque analysis into the constraint conditions. To verify the reliability of the results, sensitivity analysis and various optimization algorithms were employed to validate the results. Therefore, this research involved a comprehensive mechanical analysis, the development of mathematical models, and the resolution of the following problems.

Problem 1: With the device oscillating exclusively in response to ocean waves, using parameters such as incident wave frequency and additional pendulum mass, force analyses are conducted to calculate the oscillation displacement and velocity of the buoy and pendulum. These parameters are investigated under two conditions: constant damping coefficients and damping coefficients that vary systematically with the relative velocity of the buoy and pendulum.

Problem 2: The device continues its oscillatory motion with constant damping coefficients within a specified range. The values within this range differ, and our objective is to determine the maximum output power and the corresponding damping coefficients under two scenarios: (1) constant damping coefficients and (2) damping coefficients that vary systematically with the relative velocity of the buoy and pendulum.

Problem 3: The buoy undergoes both oscillatory and pitch motions. We use parameters to establish a mathematical model and calculate the oscillation displacement and velocity of the buoy and the pitch angle displacement and angular velocity under the conditions of constant linear and rotational damping coefficients.

Problem 4: Similarly to the description in Problem 3, the buoy simultaneously experiences oscillatory and pitch motions. However, the linear and rotational damping coefficients are constant but within a specified range. The maximum output power and the optimal damping coefficients are calculated within this range.

This research aimed to enhance the efficiency of wave energy conversion by addressing the complex dynamics and interactions within the system.[11–13] Internet of Things (IoT) devices, integrated with a variety of sensors, are used to ascertain diverse parameters and conditions of the ocean. These sensors include wireless voltmeters, wireless alternating current meters, wireless voltage detectors, wireless resistance sensors, wireless temperature sensors, wireless accelerometers, wireless pressure meters, and wireless water level sensors. They collectively

enable the real-time monitoring of ocean wave conditions via an IoT platform.[14] There is a close relationship between buoys and sensors in wave power generation systems, with sensors playing a crucial role in the monitoring and control of the system. These sensors are installed on buoys to monitor their position, orientation, and movement. Sensors can also be installed at the water surface near the buoys to monitor wave height, frequency, and direction. This information aids in optimizing the design of the power generation system to maximize the capture of wave energy. Additionally, sensors can be integrated into the power generation equipment to monitor its performance and status. These sensors can measure parameters such as rotational speed, voltage, and current of the generation equipment to ensure proper operation and necessary maintenance.[15]

We seek to contribute to the development of renewable energy sources in the face of growing energy demands and environmental concerns in the 21st century. Through these investigations, we aimed to gain a deep understanding of the mechanics and physics involved in this innovative energy conversion system. Furthermore, we sought to develop a reliable and efficient solution for harnessing ocean wave energy while addressing the complexities posed by varying conditions and parameters in a simulation.[16,17] This study was primarily focused on optimizing the design of a wave energy conversion system to address the four key problems above. First, a force analysis was conducted on the equilibrium state, which yielded the initial configuration of the entire device. Using the sea surface as the reference coordinate system, we set the initial displacements and velocities to zero. In the case of the pendulum, in its initial state, there was no relative velocity between the floater and the pendulum, the linear damper did not exert any force, and the spring force was in equilibrium with the pendulum's gravity. During motion, the pendulum encountered resistance from the damper and a newly introduced spring force. For the floater, in the initial state, the buoyant force from the seawater was in equilibrium with the total weight of the device. During the motion, the floater was subjected to various forces, including wave excitation force, additional inertial force, wave-induced damping force, and buoyancy restoring force after balancing with gravity, as well as the reactive forces from the damper and the spring. The motion models of the floater and the pendulum were established on the basis of Newton's second law, resulting in a system of second-order ordinary differential equations with displacement as the unknown variable.

To enhance precision in solving the model, the equations were transformed into a system of first-order ordinary differential equations by introducing velocity variables. To ensure accuracy in the results, the Euler-predictor-corrector method with second-order accuracy was used to solve the equations.[18] These models were programmed and solved for two different scenarios pertaining to Problem 1. Problem 2 involved the optimization of the PTO system's energy output, which was governed by the work done by the linear damper. Using the equation power = force × velocity, we calculated the instantaneous power, and subsequently, the average power over a certain time interval could be obtained through integration. With the objective of maximizing the average power expressed as an integral and using the damping coefficient as the decision variable, subject to the motion equations established in Problem 1, we created an optimization model for maximizing power output. During the model-solving process, the integral in the average power expression was computed using the trapezoidal rule. In practical

implementation, the system's motion equations were first simulated for a period T_0, allowing the system to exhibit periodic behavior. Subsequently, the average power was computed within the time interval $[T_0, T_0 + T]$.

To solve the optimization model, it was transformed into an unconstrained minimization problem in terms of the damping coefficient. MATLAB's fminsearch[19] or fmincon[20] functions were employed to solve the model, and the optimization process typically took only a few seconds. The third optimization challenge pertained to modeling the pendulum motion, building upon the foundation laid in Problem 1. When considering the presence of pitching motion, where the directions of gravity and buoyancy form angles with the pendulum's axis, the model needs to account for the influence of the effects of gravity and buoyancy on these angles. For pitching motion, in addition to the various torques directly provided in the problem statement, the model also considered the torques generated by the vertical-axis components of gravity and buoyancy forces. Following the analysis of forces and torques, a coupled system of ordinary differential equations was established on the basis of Newton's second law for linear and angular displacements for both the pendulum and the floater, taking into account pendulum and floater rotational inertias. The equations were solved by the Euler predictor-corrector method. Through programming implementation, simulations were carried out for the parameter scenarios provided in Problem 3.

The fourth optimization challenge could be approached by modeling and solving it in a manner similar to Problem 2. In this case, the objective function for calculating average power was extended to include the contribution of the rotational damper. The decision variables consisted of two damping coefficients, one for the linear damper and one for the rotational damper, with the constraints based on the model from Problem 3. This approach enabled the use of the fmincon function to find the maximum output power. By incorporating the rotational damper into the optimization model, it became possible to address the enhanced design of the PTO system, optimizing its performance to harness wave energy more efficiently. This optimization process is aimed at striking a balance between the linear and rotational dampers to maximize power extraction from the oscillating motion of the floater and pendulum.

2. Simulation Processes

The relative motion between these two components drives the damper to perform work, which is then captured as energy output. To achieve this, mechanical analysis and mathematical modeling were conducted to address the following issues:

Issue 1: Analysis of the equilibrium state, initial configurations, and force considerations in the system.

Issue 2: Optimizion of the power output by considering the linear damper's contribution and the damping coefficient as a decision variable.

Issue 3: Modeling of the pendulum motion, incorporating the influence of angles on the strength of the effects of gravity and buoyancy during pitching motion.

Issue 4: Extension of the optimization to include the contribution of the rotational damper, with the goal of maximizing output power.

In the initial state, the entire apparatus was in equilibrium. For the pendulum, the equilibrium was governed by the balance between gravity and spring force, resulting in a two-force equilibrium. In the case of the floater, equilibrium was achieved through the balance between gravity and buoyancy, also forming a two-force equilibrium. During motion, the pendulum experienced the forces of gravity, spring force, and damping force from a linear damper. The spring force was related to displacement, while the damping force was related to velocity, leading to the formulation of a first-order differential equation with respect to time. For the floater, the situation was more complex owing to the influence of seawater. It was subjected to six forces: wave excitation force, additional inertia force, wave damping force, static water restoring force, spring force, and damping force from a linear damper. The additional inertia force was related to acceleration, and by applying Newton's second law of motion, a second-order differential equation with respect to time was derived. Solving this system of differential equations provided the oscillatory displacement and velocity of both the floater and pendulum at different time points. In Problem 2, the power calculation formula was derived from the equation power = force × velocity, and an optimization model was established. As indicated in Problem 1, the motion exhibited periodicity. The optimal solution within one period was determined, and through sensitivity analysis, the stability of the results was verified.

For Problems 3 and 4, in which pitch motion was introduced in addition to the oscillatory motion along the central axis for the floater and pendulum, we made slight modifications to the model established in Problem 1. For the pitch motion, where an angle was formed between the gravitational force and the pendulum's oscillation direction, we needed to extend the model from Problem 1. This involved conducting force and torque analyses to establish a new model. The equations of pitch motion for the pendulum and floater were derived on the basis of Newton's second law for angular displacement. In Problem 4, the objective remained the determination of maximum average power. Building upon the model developed in Problem 2, we additionally considered the output power from a rotational damper. Intelligent algorithms were employed for solving the above problems, and the stability of the results was verified through sensitivity analysis. The following were assumed in the model.

1. The masses of the spring, damper, floater compartment, and central axis can be disregarded.
2. The various frictional effects at the connections between components are negligible.
3. The floater is a thin-walled structure with mass uniformly distributed over the surface, and surface thickness need not be considered.
4. The pendulum is a solid cylinder with a uniform mass distribution (constant density).

3. Results and Discussion

3.1 Establishment and solution of model for Problem 1

In the equilibrium state, as shown in Fig. 1(a), the entire wave energy device experiences only vertical gravity and seawater buoyancy. The force balance relationship is expressed as

$$m_{total} \times g = \rho \times g \times V_d, \tag{1}$$

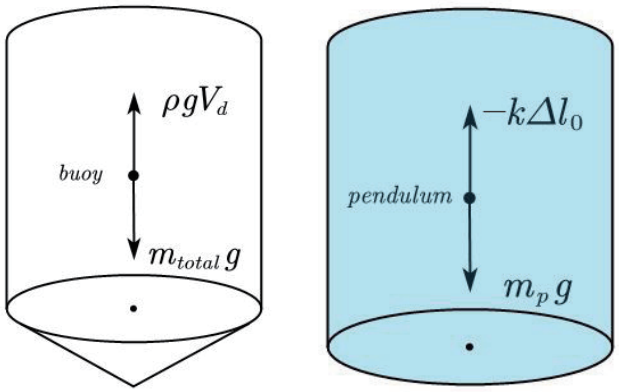

(a) (b)

Fig. 1. (Color online) Force analysis of the equilibrium state of wave energy device: (a) buoyancy force analysis and (b) pendulum force analysis.

where $m_{total} = m_b$ (mass of buoy) + m_p (mass of pendulum) = 7299 kg is the total mass of the wave energy device, ρ = 1025 kg/m^3 is the density of seawater, g = 9.8 m/s^2 is the acceleration due to gravity, and V_d is the displaced volume of the entire wave energy device (volume submerged in water). Substituting the given values, the displaced volume is calculated as $V_d = m_{total}/\rho$ = 7.12096 m^3.

On the other hand, the volume of the conical shell portion of the buoy is

$$V_c = 1/3 \times \pi \times h_c = 0.83776 \text{ m}^3, \tag{2}$$

where r_f = 1.0 m is the bottom radius of the buoy and h_c = 0.8 m is the height of the conical shell portion of the buoy. Since $V_d > V_c$, the conical shell portion of the buoy is completely submerged in seawater, as is a portion of the cylindrical shell. Let h_c denote the height of immersion of the cylindrical shell into the water, then

$$h_c = \left(V_d - V_c\right) / \pi r_f^2 = 2.00 \text{ m}. \tag{3}$$

Because of the fact that the damping force of the linear damper is proportional to the relative velocity between the buoy and the pendulum, in the initial equilibrium state, there is no relative motion between the buoy and the pendulum, and therefore, the damping force is zero. Thus, in the equilibrium state, as shown in Fig. 1(b), the pendulum experiences only the gravitational force and the spring force in the vertical direction. The force balance relationship is expressed as

$$m_p g = -k \times \Delta l_0, \tag{4}$$

where m_p = 2433 kg is the mass of the pendulum, k = 80000 N/m is the spring stiffness, and Δl_0

is the spring extension in the equilibrium state. The negative sign on the right side indicates that the direction of the spring force is opposite to the direction of extension. The extension is calculated as

$$\Delta l_0 = -m_p \times g / k = -0.2980425 \text{ m}. \tag{5}$$

Therefore, the initial length l_0 of the spring in the equilibrium state is

$$l_0 = l + \Delta l_0 = 0.5 - 0.2980425 = 0.2019575 \text{ m}, \tag{6}$$

where l = 0.5 m is the original length of the spring. Establishing the mathematical model of the oscillating motion is accomplished with the reference frame of the earth (or sea surface).

Taking the initial positions of the buoy and pendulum as their respective equilibrium positions, let their vertical displacements be denoted as $x_b(t)$ and $x_p(t)$, where upward is considered the positive direction (i.e., upward motion has positive displacement). Acceleration (a) and velocity (v) can be obtained by taking the derivatives of displacement with respect to time (t), that is, $a = \ddot{x}$ and $v = \dot{x}$. Here, a dot above x represents a first-order time derivative, and two dots represent a second-order time derivative. During the motion of the pendulum, it is subjected to three forces: gravity ($-m_p \times g$), spring force [$-k(\Delta l_0 + (x_p - x_b)$], and damping force from the linear damper [$-d_d\ (x_p - x_b)$]. Here, d_d represents the damping coefficient of the damper. The force analysis is depicted in Fig. 2(a), and according to Newton's second law, where the initial conditions are $x_p(0) = 0$ and $x_b(0) = 0$, the motion equation is given by

$$m_p \times \ddot{x}_p = -m_p \times g - k(\Delta l_0 + \left(x_p - x_b\right) - d_d\left(\dot{x}_p - \dot{x}_b\right) = -k\left(x_p - x_b\right) - d_d\left(\dot{x}_p - \dot{x}_b\right). \tag{7}$$

During the motion of the buoy, it is subjected to six forces: wave excitation force $f\cos\omega t$, additional inertia force $-m_a \times \ddot{x}_f$, wave-induced damping force $-d_w\dot{x}_b$, static buoyancy force (the difference between total buoyancy and total gravity) $-\rho \times g \times \pi \times r_f^2 \times x_b$, spring force newly

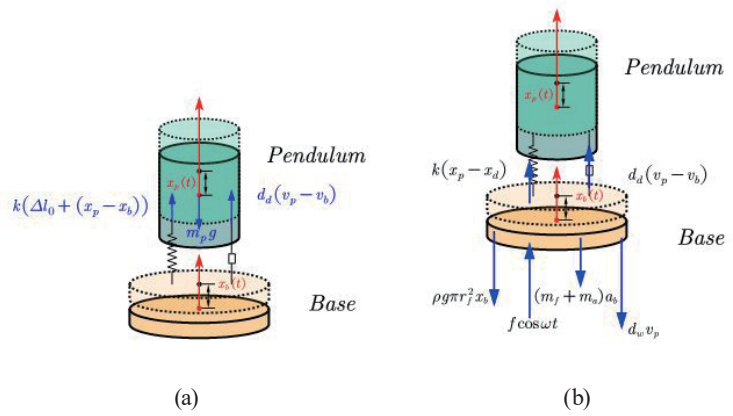

Fig. 2. (Color online) Force analyses of the motion processes for (a) the buoy, b, and (b) the pendulum, p.

generated relative to the equilibrium position $k(x_p - x_b)$ resulting from the relative displacement between the pendulum and the buoy, and damping force from the linear damper $d_d(x_p - x_b)$. The force analysis is illustrated in Fig. 2(b), where f is the amplitude of the wave excitation force, ω is the incident wave frequency, m_a is the oscillatory added mass, and d_w is the wave-induced damping coefficient. On the basis of Newton's second law, the motion equation for the buoy is

$$\left(m_f + m_a\right)\ddot{x}_b = f\cos\omega t - d_w\dot{x}_b - \rho\times g\times\pi\times r_f^2\times x_b + k\left(x_p - x_b\right) + d_d\left(\dot{x}_p - \dot{x}_b\right), \tag{8}$$

where the initial conditions are $x_b(0) = 0$ and $\dot{x}_b(0) = 0$ and the mass of the buoy is 4866 kg. In summary, the motion model for the buoy and the pendulum is

$$\begin{aligned} m_p\times\ddot{x}_b(t) &= -k\left(x_p - x_b\right) - d_d\left(\dot{x}_p - \dot{x}_b\right), \\ \left(m_f + m_a\right)\ddot{x}_f(t) &= f\cos\omega t - d_w\dot{x}_b - \rho\times g\times\pi\times r_f^2\times x_b + k\left(x_p - x_b\right) + d_d\left(\dot{x}_p - \dot{x}_b\right) = 0, \end{aligned} \tag{9}$$

where the initial conditions are $x_b(0) = 0$, $\dot{x}_b(0) = 0$, $x_p(0) = 0$, and $\dot{x}_p(0) = 0$.

The parameters for the model of Problem 1 are shown in Table 1. When the wave circular frequency is ω, the time for one wave period is $2\pi/\omega$. For Problem 1, considering only 40 wave periods, the total simulation time is chosen as $T = 40\times 2\pi/\omega \approx 180$ s. Within the interval [0, T], with a time step of $\Delta t = 0.01$ s, a uniform grid is created for time discretization, where the discrete time points are denoted as $t^n = n\Delta t$ and the corresponding displacement is $x(t^n) = x^n$, where $T/\Delta t = 18000$ and $n = 0, 1,\ldots, N$. By introducing the velocity variable $v = x$, the control equation can be equivalently transformed as follows:

$$\begin{aligned} m_p\times_p v(t) &= -k\left(x_p - x_b\right) - d_d\left(v_p - v_b\right) \\ \left(m_f + m_a\right)v_b(t) &= f\cos\omega t - d_w v_b - \rho\times g\times\pi\times r_f^2\times x_b + k\left(x_p - x_b\right) + d_d\left(v_p - v_b\right) = 0, \end{aligned} \tag{10}$$

where $\dot{x}_p(t) = v_p$, $\dot{x}_b(t) = v_b$, $x_p(0) = 0$, $v_p(0) = 0$, $x_b(0) = 0$, and $v_b(0) = 0$. To ensure the reliability of the computational results, we employ the Euler-predictor-corrector scheme to discretize the aforementioned system of ordinary differential equations.[21] The discretization format for the prediction steps are

Table 1
Parameters in model for Problem 1.

Parameter	Incident wave frequency ω (s^{-1})	Oscillatory added mass m_a (kg)	Oscillatory wave damping coefficient d_w (Ns/m)	Oscillatory excitation force amplitude f (N)
Value	1.4005	1335.535	656.3616	6250

$$\begin{aligned} v_p^* &= v_p^n + \Delta t f_1\left(t^n, x_p^n, x_b^n, v_p^n, v_p^n\right), \\ v_p^* &= v_p^n + \Delta t f_2\left(t^n, x_p^n, x_b^n, v_p^n, v_p^n\right), \\ x_p^* &= x_p^n + \Delta t f_3\left(t^n, x_p^n, x_b^n, v_p^n, v_p^n\right), \\ x_p^* &= x_p^n + \Delta t f_4\left(t^n, x_p^n, x_b^n, v_p^n, v_p^n\right), \end{aligned} \tag{11}$$

and the correction steps are

$$\begin{aligned} v_p^{(n+1)} &= v_p^n + 0.5\Delta t\left[f_1\left(t^n, x_p^n, x_b^n, v_p^n, v_p^n\right) + f_1\left(t^{n+1}, x_p^*, x_b^*, v_p^*, v_p^*\right)\right], \\ v_b^{(n+1)} &= v_b^n + 0.5\Delta t\left[f_2\left(t^n, x_p^n, x_b^n, v_p^n, v_p^n\right) + f_2\left(t^{n+1}, x_p^*, x_b^*, v_p^*, v_p^*\right)\right], \\ x_p^{(n+1)} &= x_p^n + 0.5\Delta t\left[f_3\left(t^n, x_p^n, x_b^n, v_p^n, v_p^n\right) + f_3\left(t^{n+1}, x_p^*, x_b^*, v_p^*, v_p^*\right)\right], \\ x_b^{(n+1)} &= x_b^n + 0.5\Delta t\left[f_4\left(t^n, x_p^n, x_b^n, v_p^n, v_p^n\right) + f_4\left(t^{n+1}, x_p^*, x_b^*, v_p^*, v_p^*\right)\right], \end{aligned} \tag{12}$$

where

$$\begin{aligned} & x_b^0 = v_b^0 = x_p^0 = v_p^0 = 0, \\ & f_1\left(t, x_p, x_b, v_p, v_b\right) = \left[-k\left(x_p - x_b\right) - d_d\left(v_p - v_b\right)\right] / m_p, \\ & f_2\left(t, x_p, x_b, v_p, v_b\right) \\ & \quad = \left[f\cos\omega t - d_w v_b - \rho \times g \times \pi \times r_f^2 \times x_b + k\left(x_p - x_b\right) + d_d\left(v_p - v_b\right)\right] / \left(m_p + m_b\right), \\ & f_3\left(t, x_p, x_b, v_p, v_b\right) = v_p, \\ & f_4\left(t, x_p, x_b, v_p, v_b\right) = v_b. \end{aligned} \tag{13}$$

3.1.1 d_d is 10000 N·s/m

MATLAB programming was utilized to solve and obtain the oscillation displacement and velocity curves for the buoy and pendulum, as shown in Fig. 3. The reference points for the oscillation displacement and velocity curves of the buoy are the initial position points, and the two curves exhibit extremely high similarity. As time progresses, the extreme values of the oscillatory displacement and velocity of the buoy gradually stabilize at approximately 0.43 m and 0.6 m/s, respectively, and eventually exhibit periodic variations after a certain duration. Similarly, the oscillation displacement and velocity curves for the pendulum, with the buoy as the reference object, also demonstrate a high degree of similarity. Over time, the relative oscillation displacement and velocity extremes of the pendulum with respect to the buoy gradually stabilize at approximately 0.025 m and 0.038 m/s, respectively, and exhibit periodic variations after a certain duration. Table 2 provides the oscillation displacement and velocity of the buoy and pendulum at time intervals of 10, 20, 40, 60, and 100 s.

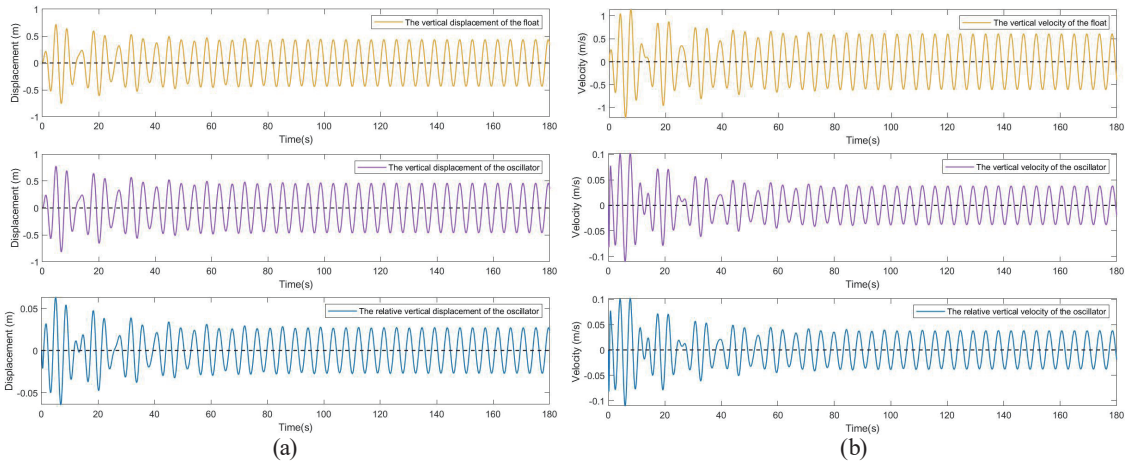

(a) (b)

Fig. 3. (Color online) Computational results for scenario 1 of Problem 1: (a) oscillation displacement curves of the buoy and pendulum and (b) oscillation velocity curves of the buoy and pendulum.

Table 2
Oscillation displacement and velocity of the buoy and pendulum in scenario 1.

Time (s)	10	20	40	60	100
Buoy oscillation displacement x_f (m)	−0.19703	−0.59289	0.28848	−0.31922	−0.08965
Buoy velocity v_f (m/s)	−0.63652	−0.22854	0.30792	−0.47276	−0.60230
Pendulum oscillation displacement x_p (m)	−0.21847	−0.63673	0.29981	−0.33651	−0.09049
Pendulum velocity v_p (m/s)	−0.68897	−0.25942	0.32771	−0.50865	−0.64106

3.1.2 $d_d = 10000|v_p - v^b|^{0.5}$ N·s/m

We also employed MATLAB programming to solve and obtain the oscillation displacement and velocity curves for the buoy and pendulum. As illustrated in Fig. 4, we observed that even with varying damping coefficients, the results obtained were highly similar to those in scenario 1. Table 3 provides the oscillation displacement and velocity of the buoy and pendulum at time intervals of 10, 20, 40, 60, and 100 s.

3.2 Establishment and solution of model for Problem 2

From Problem 2, it is known that the energy output of the PTO system is the work done by the linear damper. According to the modeling process in Problem 1, it is known that the damper bears a damping force of $d_d(v_p - v_b)$. Under this force, the displacement of the damper is $(x_p - x_b)$, and the deformation velocity of the damper is $(v_p - v_b)$. According to the equation power = force × velocity, the instantaneous power P of the damper is $d_d(v_p - v_b)^2$. The average output power P during the time interval $[T_0, T_0 + \Delta T]$ is calculated as

$$\overline{P} = \frac{1}{\Delta T}\int_{T_0}^{T_0+\Delta T} d_d \left(v_p - v_b\right)^2 dt. \tag{14}$$

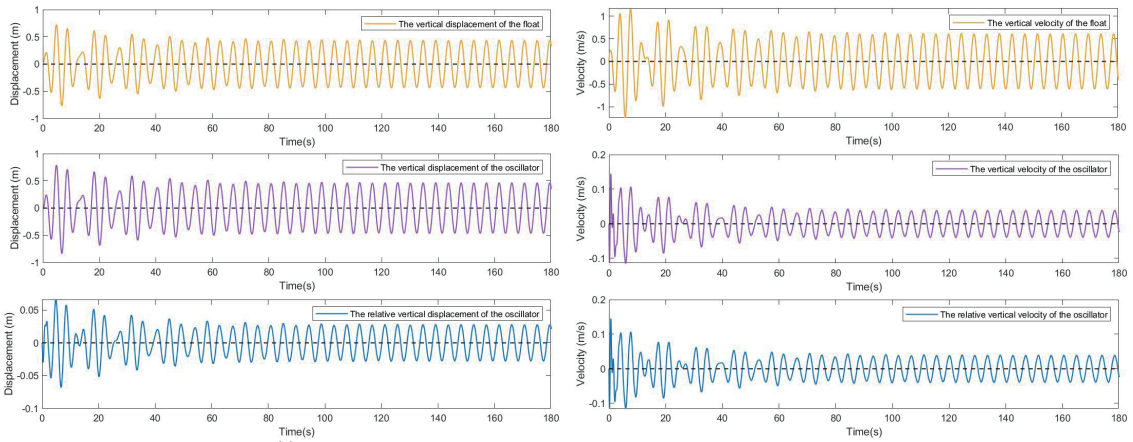

(a) (b)

Fig. 4. (Color online) Computational results for scenario 1 of Problem 2: (a) oscillation displacement curves of the buoy and pendulum and (b) oscillation velocity curves of the buoy and pendulum.

Table 3
Oscillation displacement and velocity of the buoy and pendulum in scenario 2.

Time (s)	10	20	40	60	100
Buoy oscillation displacement x_f (m)	−0.21227	−0.61340	0.27173	−0.33199	−0.09451
Buoy velocity v_f (m/s)	−0.64798	−0.24185	0.29078	−0.48441	−0.60775
Pendulum oscillation displacement x_p (m)	−0.24139	−0.66354	0.28329	−0.35476	−0.09999
Pendulum velocity v_p (m/s)	−0.69437	−0.26297	0.30785	−0.51793	−0.64783

Problem 2 requires optimizing the damping coefficient of the damper to maximize the average output power. Therefore, the mathematical model for this problem is expressed as follows:

$$\max\left[\overline{P}\left(d_d\right)=\frac{1}{\Delta T}\int_{T_0}^{T_0+\Delta T} d_d\left(v_p-v_b\right)^2 dt\right], \tag{15}$$

$$\begin{aligned} m_p\times\dot{v}_p\left(t\right)&=-k\left(x_p-x_b\right)-d_d\left(v_p-v_b\right),\\ \left(m_f+m_a\right)\dot{v}_b\left(t\right)&=f\cos\omega t-d_w v_b-\rho\times g\times\pi\times r_f^2\times x_b+k\left(x_p-x_b\right)+d_d\left(v_p-v_b\right)=0, \end{aligned} \tag{16}$$

where $\dot{x}_p\left(t\right)=v_p$, $\dot{x}_b\left(t\right)=v_b$, $x_p\left(0\right)=v_p\left(0\right)=x_b\left(0\right)=v_b\left(0\right)$.

For Problem 2, we will also consider two scenarios and solve the above model accordingly. For Problem 2, the parameters in the model are as follows: the incident wave frequency is 2.2143 s^{-1}, the oscillatory added mass m_a is 1165.992 kg, the oscillatory wave damping coefficient d_d is 167.8395 N·s/m, and the oscillatory excitation force amplitude f is 4890 N.

3.2.1 d_d is a constant

In the case where the damping coefficient is constant, given that the damping coefficient lies within the range [0, 100000], if the average output power is a monotonic function of the damping coefficient, an efficient solution can be obtained by the binary search method. However, from the model, it can be observed that when $d_d = 0$, $\overline{P} = 0$; and when d_d tends to infinity, there will be no relative motion between the pendulum and the float, resulting in $\overline{P} = 0$. Therefore, the average output power is not a monotonic function of the damping coefficient. In this case, using the binary search method may not lead to the optimal solution. Given these reasons, we transform the objective function equivalently to

$$\min\left[-\overline{P}\left(d_d\right)=\frac{1}{\Delta T}\int_{T_0}^{T_0+\Delta T} d_d\left(v_p-v_b\right)^2 dt\right]. \tag{17}$$

The problem is transformed into an unconstrained minimization problem with respect to the damping coefficient and then solved using optimization tools in MATLAB, such as fminsearch or fmincon. The solving process takes only a few seconds. When computing the integral in the objective function, we employ the trapezoidal rule. In the specific implementation, we first simulate the motion equations for duration T_0 to induce periodicity in the system. Subsequently, we calculate the average power over the time interval [T_0, $T_0 + T$], and the calculation is performed using the MATLAB library function fminsearch. For this scenario, with $T_0 = 100$ s and $T = 200$ s, the maximum average power is found to be 229.16 W, corresponding to an optimal damping coefficient of 37198 N·m/s. To validate the reliability of the results, Fig. 5 illustrates the variation of maximum output power with the damping coefficient. It is evident that the curve is convex, facilitating the attainment of a global optimum, and the optimal solution aligns with our computed result.

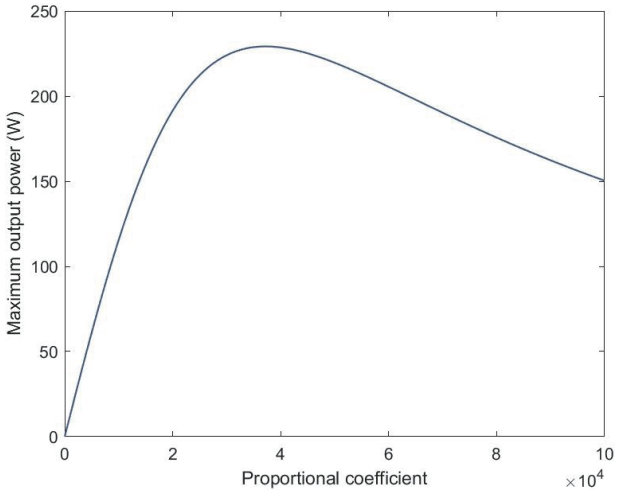

Fig. 5. Variation of maximum output power with damping coefficient in scenario 1 of Problem 2.

3.2.2 d_d is a power function of the absolute value of the relative velocity

In this scenario, the formula for calculating the damping (damping coefficient) is as follows:

$$d_d = d_0 \times \left| v_p - v_b \right|^c , \tag{18}$$

where the proportionality coefficient d_0 lies in the range [0, 100000], and the power exponent c is within the range [0, 1]. In this case, the objective function is actually given by

$$\max \left[\overline{P}\left(d_0, c\right) = \frac{1}{\Delta T} \int_{T_0}^{T_0+\Delta T} d_0 \times \left| v_p - v_b \right|^c \times \left(v_p - v_b \right) dt \right]. \tag{19}$$

In this scenario, there are actually two decision variables. When using the fminsearch function for computation, there arises an issue of the variable exceeding its range. Therefore, the fmincon function is employed to solve the problem. The obtained maximum average power is 229.16 W, corresponding to the optimal damping proportionality coefficient of 37198 and a power exponent of 6.3×10^{-7}. To verify the reliability of the computational results, we plotted a 3D graph illustrating the relationship between the maximum output power and the proportionality coefficient and power exponent of the damping factor, as shown in Fig. 6.

We observe that the obtained 3D surface is convex, indicating the existence of a maximum average power and consequently yielding a globally optimal solution. It is noteworthy that the peak of the graph is relatively flat. Therefore, when using different optimization algorithms, there may be instances where the objective function values are nearly identical, but the optimal parameter values differ significantly. Furthermore, Fig. 7 illustrates the 1D functional relationship between the maximum output power and the proportionality coefficient and power

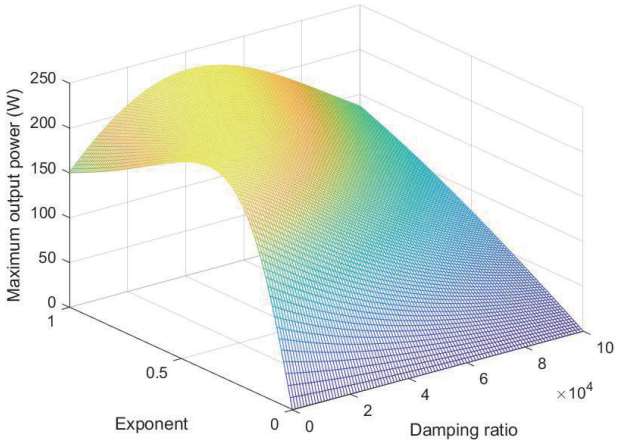

Fig. 6. (Color online) 3D plot illustrating the relationship between the maximum output power and the proportionality coefficient and power exponent of the damping factor.

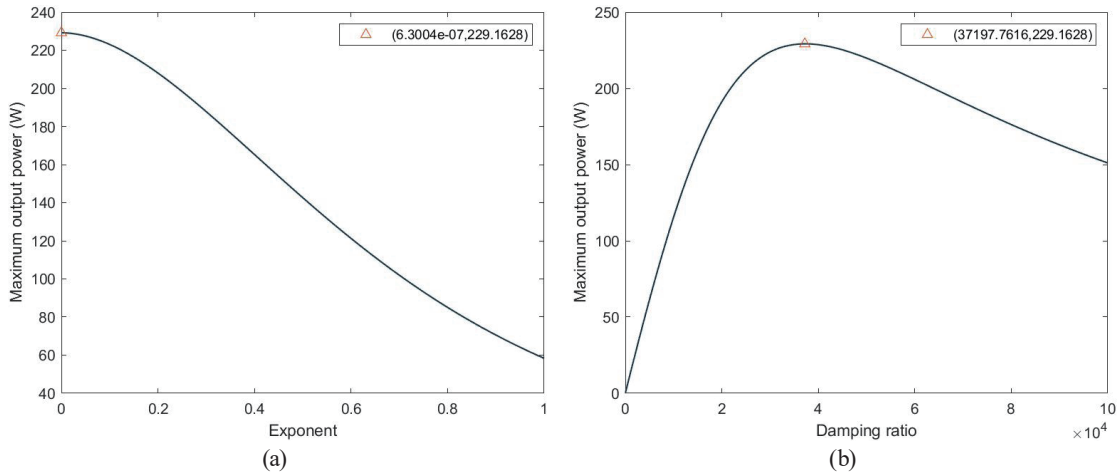

Fig. 7. (Color online) Parameter dependence of the maximum output power. (a) Variation of the maximum output power with the power exponent. (b) Variation of the maximum output power with the proportionality coefficient.

exponent. It is evident that the maximum output power decreases with decreasing power exponent. This observation helps explain why the optimal power exponent we obtained is close to 0.

Here, we analyze the sensitivity of the calculation results to the chosen interval length T. In the analysis, T_0 is set to 100 s, and different values of T are considered. Figure 8 presents the corresponding results. We observe that with the increase in interval length, the damping power exhibits periodic fluctuations and gradually stabilizes. All maximum power values are around 229, indicating that the calculation results are insensitive to T, thereby ensuring the stability of the computational results.

3.3 Establishment and solution of model for Problem 3

When analyzing the pendulum motion equation, the primary reference frame is established with respect to the earth (sea surface). Subsequently, the initial positions of the buoy and pendulum are defined as equilibrium positions, and oscillatory displacement and angular displacement are measured with reference to these positions. In the context of oscillatory motion, the variable notations employed in Problem 1 are maintained. Specifically, their displacements along the vertical direction (along the central axis direction) are denoted as $x_b(t)$ and $x_p(t)$, with corresponding velocities denoted as $v_b(t)$ and $v_p(t)$. Upward is considered the positive direction. For pitch motion considerations, their angular displacements are designated as $\theta_b(t)$ and $\theta_p(t)$, with angular velocities denoted as $w_b(t) = \theta_b(t)$ and $w_p(t) = \theta_p(t)$, and a clockwise rotation is considered as the positive direction. The oscillatory motion of the pendulum is still driven by the combined forces of spring elasticity and damping resistance, with the direction of oscillatory motion aligned along the central axis. As deduced from the modeling process in Problem 1, in the case of pure oscillatory motion, the spring force is actually given by $-k(\Delta l_0 + x_p - x_b)$. When the angular displacement of the pendulum, θ_p, is 0, the gravitational force on the pendulum,

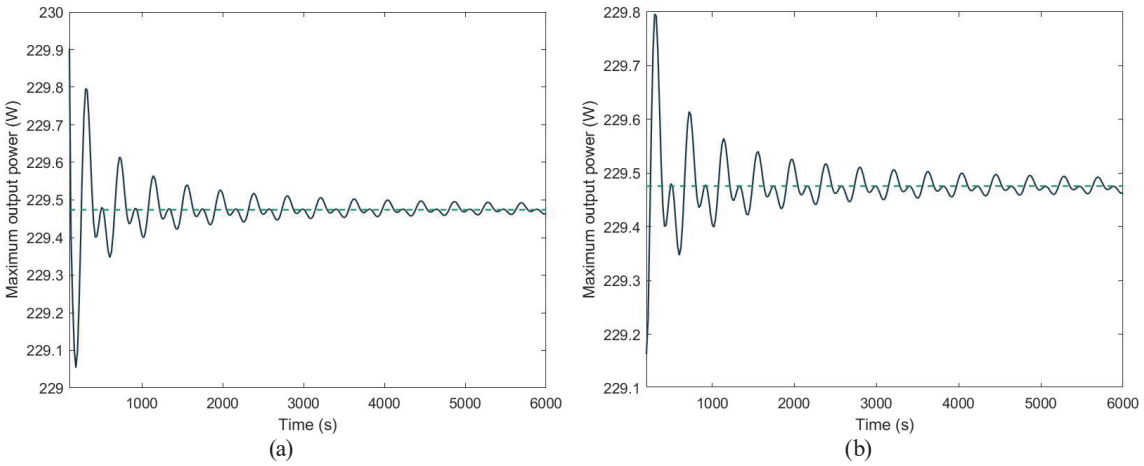

Fig. 8. (Color online) Results of sensitivity analyses regarding the interval length: (a) scenario 1 and (b) scenario 2.

$-m_p \times g$, is balanced by $-k\Delta l_0$, resulting in an effective driving force for oscillatory motion of $-k(x_p - x_b)$. However, when $\theta_p \neq 0$, an angle is formed between the gravitational force and the direction of pendulum oscillation. The component of gravity in the oscillation direction can be calculated as $-m_p \times g \times \cos(\theta_p)$. Consequently, the effective driving force for oscillatory motion becomes

$$-k\left(\Delta l_0 + x_p - x_b\right) - m_p \times g \times \cos\left(\theta_p\right) = m_p \times g \times \left(1 - \cos\left(\theta_p\right)\right) - k\left(x_p - x_b\right). \tag{20}$$

The linear damping force is the same as in Problem 1. Therefore, by drawing on the modeling approach from Problem 1, we can derive the oscillatory motion equation for the pendulum in the presence of pitch motion as shown below.

$$m_p \times \dot{v}_p\left(t\right) = m_p \times g \times \left(1 - \cos\left(\theta_p\right)\right) - k\left(x_p - x_b\right) - d_d\left(v_p\left(t\right) - v_b\left(t\right)\right) \text{ and } \dot{x}_p\left(t\right) = v_p \tag{21}$$

The rotation of the pendulum is primarily driven by the torque generated from the torsional spring, $-k_t \times (\theta_p - \theta_b)$, and the torque produced by the rotational damper, $-d_r(w_p - w_b)$, where k_t and d_r are the stiffness of the torsional spring and the damping coefficient of the rotary damper, respectively. Additionally, the gravitational component along the vertical central axis direction exerts a torque that drives the rotation. The formula for calculating this torque is given by $m_p \times g \times \sin(\theta_p) \times L_p$. Therefore, on the basis of Newton's second law, the equation of motion for the pendulum in pitch motion is obtained as

$$I_p \times \dot{w}_p\left(t\right) = m_p \times g \times \sin\left(\theta_p\right) \times L_p - k_t \times \left(\theta_p - \theta_b\right) - d_r\left(w_p - w_b\right) \text{ and } \dot{\theta}_p = w_p, \tag{22}$$

where I_p is the moment of inertia of the pendulum. The initial conditions for the above motion equation are $x_p(0) = 0$, $v_p(0) = 0$, $\theta_p(0) = 0$, and $w_p(0) = 0$.

For the pitch motion, it is noteworthy that the rotation of the buoy occurs around the center of buoyancy (the intersection point of the central axis and the horizontal plane). As analyzed in Problem 1, the distance from the center of buoyancy to the apex of the cone when in the equilibrium state is $h_d + h_c = 2.8$ m, where h_d and h_c are the dipping length and cone shell length, respectively. Therefore, during motion, the distance from the center of buoyancy to the apex is $(2.8 - x_b)$ m. Additionally, to calculate the moment of inertia for the rotation of the float, it is necessary to determine the position of its center of mass. Since the mass of the buoy is distributed over the surface, determining the center of mass requires the calculation of the surface area. For the cone shell and the cylindrical shell (considering the top cover), their surface areas are, respectively,

$$S_{col} = \pi r_b \sqrt{h_{shell}^2 + r_{shell}^2} \text{ and } S_{con} = 2\pi r_b h_{con} + \pi, \tag{23}$$

where S_{col}, S_{con}, and h_{con} are the surface area of the cone shell, surface area of the cylinder, and height of the cylinder. The distance from the centroid to the apex of the cone can be determined from them, as shown below.

$$h_{con} + 0.5\left(S_{con} - S_{col}\right) / \left(2\pi r_b\right) = h_{con} + 0.5\left(h_{con} - 0.5\sqrt{h_{shell}^2 + r_{shell}^2} + 0.5r_b\right) = 2.2298 \tag{24}$$

Thus, the distance between the center of gravity and rotational center point of the buoy can be obtained.

$$L_b = \left(2.8 - 2.2298\right) - x_b = 0.5702 - x_b \tag{25}$$

It can also be determined that the rotational inertia of the buoy is $I_b = m_b L_b^2$. For Problem 3, the parameters in the model are as follows: the incident wave frequency is 1.7152 s^{-1}, the oscillatory added mass m_a is 1028.876 kg, the oscillatory wave damping coefficient d_d is 683.4558 N s/m, the oscillatory excitation force amplitude f is 3640 N, the pitch added moment of inertia I_a is 7001.914 kg·m², the pitch wave damping coefficient d_p is 654.3383 Nms, and the pitch excitation moment amplitude L is 1690 N·m. When the wave circular frequency is ω, the time for one wave period is $2\pi/\omega$. For Problem 3, only 40 wave periods are considered, so the total simulation time is taken as $T = 40 \times 2\pi/\omega \approx 146.5$ s. Here, the Euler-predictor-corrector scheme continues to be used to solve this model. Because of the complexity of the model, it is not convenient to provide the discrete format. We have obtained the oscillatory displacement curves for the buoy and pendulum, as well as the oscillatory velocity curves, pitch angle displacement curves, and pitch angular velocity curves, as shown in Fig. 9. Detailed results are presented in Table 4.

From the above calculation results, it can be seen that the buoy and pendulum rotate almost synchronously, and their rotational amplitudes are nearly identical. This may be attributed to an overly rigid connection between the buoy and pendulum, namely, an excessively high torsional spring stiffness. To validate our hypothesis, we reduced the torsional spring stiffness from

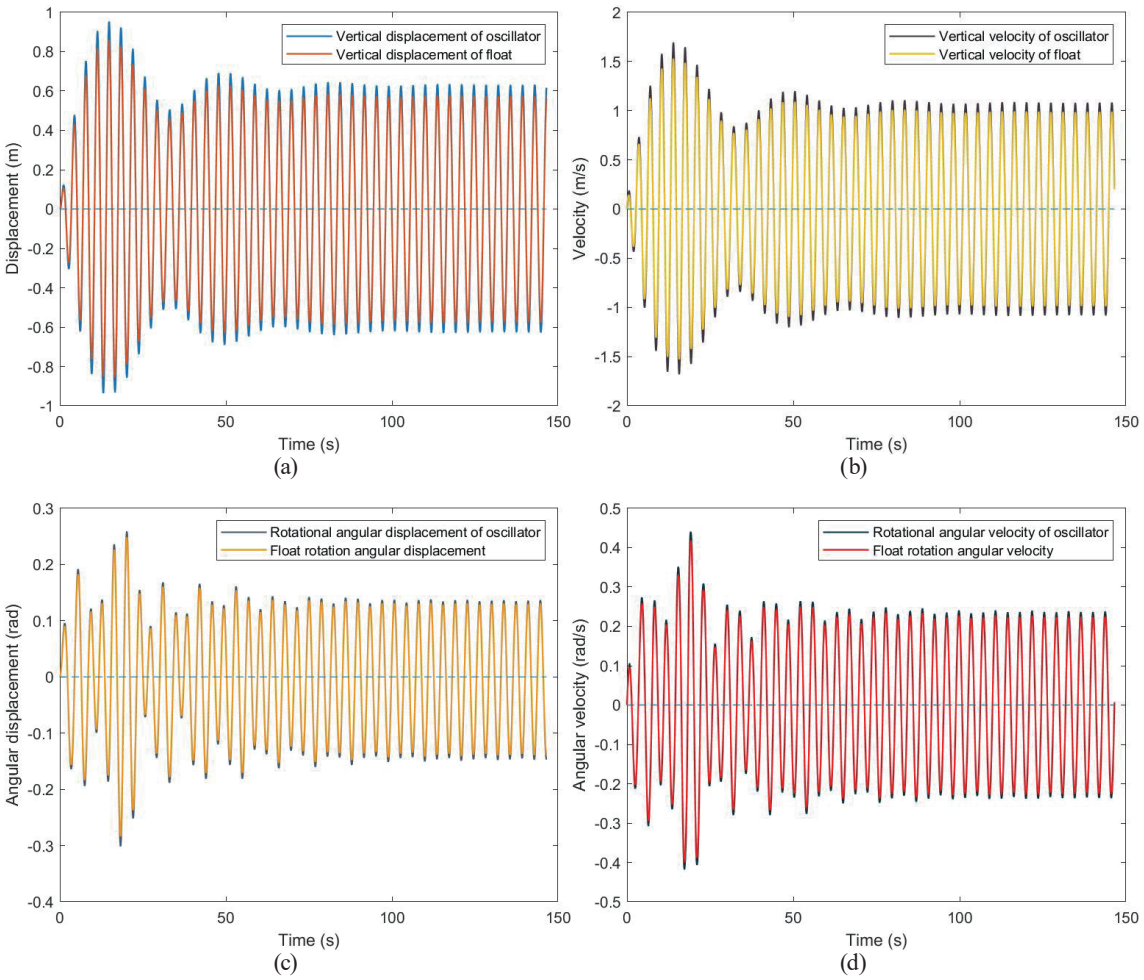

Fig. 9. (Color online) Computational results for Problem 3 (torsional spring stiffness is 250000): (a) oscillatory displacement curve of the buoy and pendulum, (b) oscillatory velocity curve of the buoy and pendulum, (c) pitch angle displacement curve of the buoy and pendulum, and (d) pitch angular velocity curve of the buoy and pendulum.

Table 4
Oscillatory displacement and velocity of the buoy and pendulum, and pitch angle displacement and angular velocity.

Time (s)	10	20	40	60	100
Buoy oscillatory displacement x_b (m)	–0.55198	–0.75425	0.35870	–0.35160	–0.05554
Buoy velocity v_v (m/s)	0.96684	–0.41629	0.70467	–0.76841	–0.97396
Buoy angular displacement θ_b (Tad)	0.04549	0.23791	–0.14155	0.08640	0.03858
Buoy angular velocity w_b (Tad/s)	–0.18799	0.12651	–0.0721	0.13581	0.21637
Pendulum oscillatory displacement x_p (m)	–0.62418	–0.81647	0.38400	–0.37476	–0.04844
Pendulum velocity v_p (m/s)	1.02760	–0.46095	0.78928	–0.84853	–1.06690
Pendulum angular displacement θ_p (Tad)	0.04738	0.24807	–0.14903	0.09055	0.04057
Pendulum angular velocity w_p (Tad/s)	–0.19571	0.13074	–0.07811	0.14158	0.22072

250000 to 25000 and performed the calculations again. The results are shown in Fig. 10. At this point, the oscillatory displacement and velocity of the pendulum and buoy remain unchanged. However, the pitch amplitude of the pendulum is significantly larger than that of the buoy, consistent with the animation of Problem 2, thereby confirming the validity of the model presented in this paper.

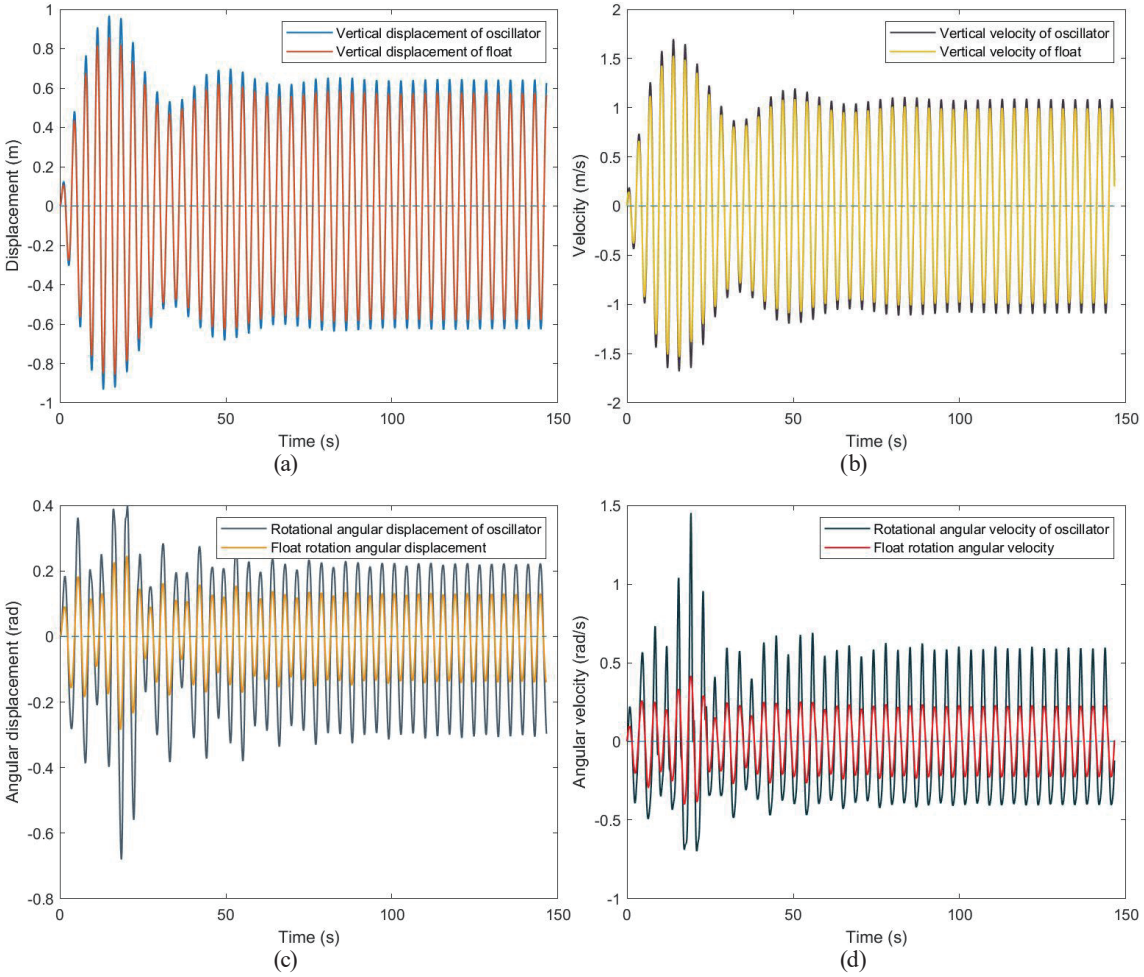

Fig. 10. (Color online) Computational results for Problem 3 (torsional spring stiffness is 25000): (a) oscillatory displacement curve of the buoy and pendulum, (b) oscillatory velocity curve of the buoy and pendulum, (c) pitch angle displacement curve of the buoy and pendulum, and (d) pitch angular velocity curve of the buoy and pendulum.

3.4 Establishment and solution of model for Problem 4

Problem 4 requires further consideration of the output power of the rotational damper, judging from the analysis for Problem 2. As revealed in the modeling process for Problem 3, the damping torque generated by the rotational damper is given by $d_r \times (w_o - w_b)$. Under the influence of this torque, the rotational damper undergoes an angular displacement of $\theta_o - \theta_b$, and the angular deformation velocity of the damper is given by $w_o - w_b$. Applying the principle of rotational power = torque × angular velocity, the instantaneous power of the rotational damper is expressed as $d_r \times (w_p - w_b)^2$. Over the time interval $[T_0, T_0 + T]$, the overall average output power P can be defined as follows.

$$P = \frac{1}{T}\int_{T_0}^{T_0+T}\left[d_d \times \left(v_p - v_b\right)^2 + d_r \times \left(w_p - w_b\right)^2\right]dt \tag{26}$$

Problem 4 requires the optimization of the damping coefficients of the linear damper and rotational damper to maximize the average output power. Therefore, the mathematical model for this problem is as follows.

$$\max \overline{P}\left(d_d, d_o\right)\frac{1}{T}\int_{T_0}^{T_0+\Delta T}\left[d_d \times \left(v_p - v_b\right)^2 + d_r \times \left(w_p - w_b\right)^2\right]dt, \tag{27}$$

$$\begin{aligned}
m_p \times v_p(t) &= m_p \times g \times \left(1-\cos\left(\theta_p\right)\right) - k\left(x_p - x_b\right) - d_d\left(v_p(t) - v_b(t)\right),\\
I_p \times w_p(t) &= m_p \times g \times \sin\left(\theta_p\right) \times L_p - k_t \times \left(\theta_p - \theta_b\right) - d_r\left(w_p - w_b\right),\\
\left(m_b + m_a\right) \times v_p(t) &= f\cos\omega t - d_d \times v_b\\
&\quad -\rho \times g \times \pi \times r_b^2 \times x_b \times \cos\left(\theta_p\right) m_p \times g \times \left(1-\cos\left(\theta_p\right)\right)\\
&\quad +k\left(x_p - x_b\right) - d_d\left(v_p - v_b\right),\\
\left(I_b + I_a\right) \times w_b(t) &= L \times \cos\omega t - d_p \times w_b - k_s\theta_b + \rho \times g \times \pi \times r_b^2 \times x_b \times \sin(\theta_p) \times L_p,\\
x_p(t) &= v_p,\ \theta_p(t) = \omega_p,\ x_b(t) = v_b,\ \theta_b(t) = \omega_b,\\
x_p(0) &= v_p(0) = \theta_p(0) = w_p(0) = x_b(0) = v_b(0) = \theta_b(0) = w_b(0) = 0.
\end{aligned} \tag{28}$$

k_s is the static water restoring moment coefficient. For Problem 4, the parameters in the model are as follows: the incident wave frequency is 1.9806 s^{-1}, the oscillatory added mass m_a is 1091.099 kg, the oscillatory wave damping coefficient d_d is 528.5018 N m/s, the oscillatory excitation force amplitude f is 1760 N, the pitch added moment of inertia I_a is 7142.493 kg·m², the pitch wave damping coefficient d_d is 1655.909 N m/s, and the pitch excitation moment amplitude L is 2140 N·m. Figure 11 illustrates the 3D relationship between the maximum output power, rotational damping coefficient, and linear damping coefficient. As can be seen, the obtained 3D surface remains convex, indicating the existence of a maximum average power. The optimization algorithm easily yields a globally optimal solution. The final result reveals a maximum output

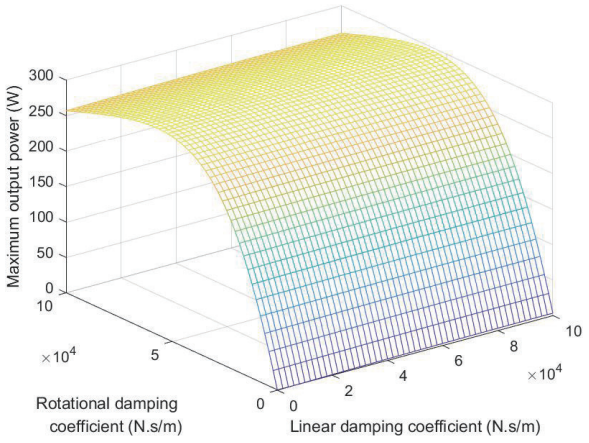

Fig. 11. (Color online) 3D relationship between the maximum output power and the rotational damping coefficient and linear damping coefficient.

power of 294.8583 W, with corresponding optimal values for the rotational damping coefficient at 99999.9199 N m/s and the linear damping coefficient at 56957.96676 N·m/s.

To verify the reliability of the results, we conducted result validation using both the quantum genetic algorithm[22] and the improved flower pollination algorithm (tMFPA).[23] Figure 12 illustrates the convergence process of the quantum genetic algorithm, while Fig. 13 shows the results obtained through the tMFPA algorithm. It is noteworthy that the computational outcomes from these various methods are consistent, thereby validating the reliability of the results. This multi-algorithm validation approach enhances the robustness and credibility of the findings. The tMFPA algorithm utilizes chaotic mapping for the initialization of the positions of individual flowers. Subsequently, during the global pollination process, individual positions are updated by leveraging random individuals with t-distribution perturbations and Levy flights. This

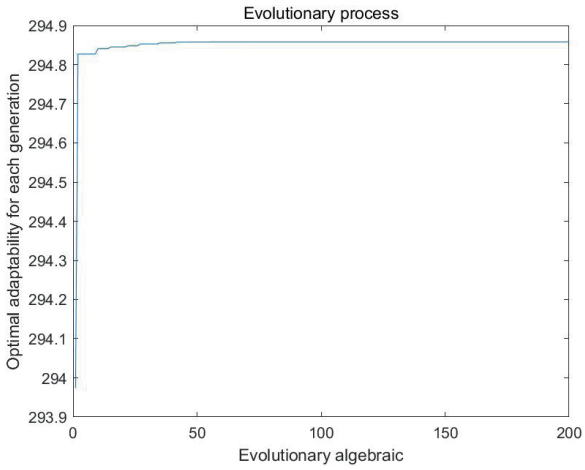

Fig. 12. (Color online) Convergence process of the quantum genetic algorithm.

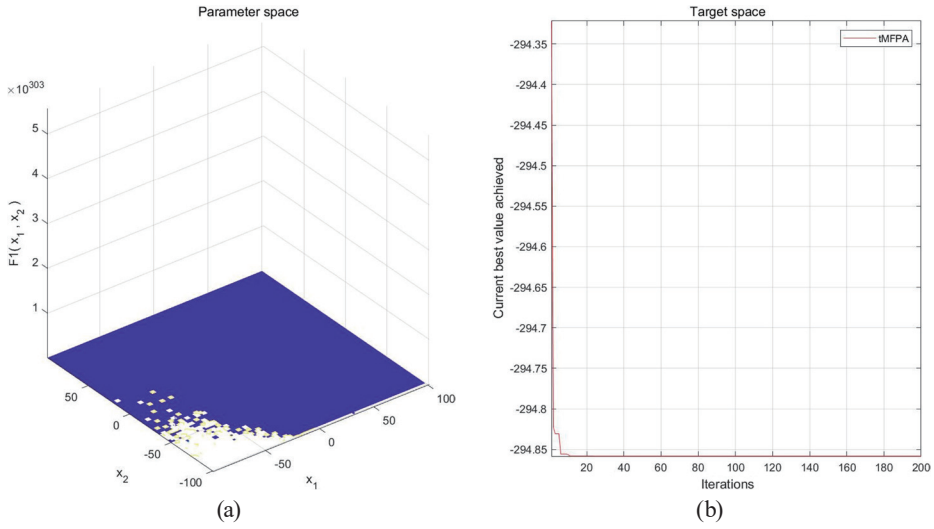

Fig. 13. (Color online) Schematic diagram of flower pollination algorithm: (a) parameter space composed of two differential vectors and (b) gradual convergence of the objective function.

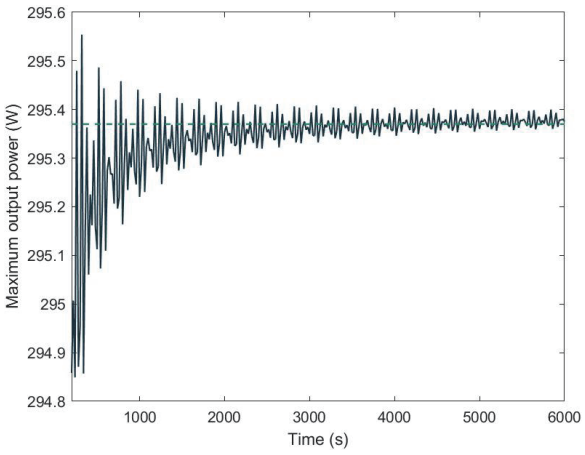

Fig. 14. (Color online) Sensitivity analysis for Problem 4.

collaborative approach accelerates convergence and enhances the diversity of the search space. In the local pollination process, the algorithm incorporates a mutation strategy with two differential vectors and a low-probability strategy to facilitate escaping from local optima.

Within the algorithm, the expression for maximum power output is employed as the fitness function for tMFPA, aiming to determine the maximum power output value. Figure 13(a) illustrates the parameter space composed of two differential vectors, while Fig. 13(b) demonstrates the gradual convergence of the objective function with increasing iteration counts. The algorithm ultimately achieves a maximum power output value of 294.8583 W. This comprehensive approach combines chaotic initialization, global pollination with t-distribution perturbations and Levy flights, and local pollination with a mutation strategy, contributing to the efficiency of the tMFPA algorithm in finding optimal solutions in the context of maximum power output. Similar to Problem 2, we conducted a sensitivity analysis on the results, and the findings are presented in Fig. 14. Upon analysis, we observed a satisfactory level of result stability, meeting our expectations.

4. Conclusions

For Problem 1, we established a motion model for the buoy and pendulum on the basis of complex oscillatory motion and simplified the problem. Newton's second law was applied, taking into account the damping forces of gravity, spring force, and the linear damper during the pendulum motion. Additionally, the buoy experienced six forces (wave excitation force, added inertia force, wave damping force, static water restoring force, spring force, and linear damper force) from the seawater, enhancing the accuracy and reliability of the model. The Euler-predictor-corrector scheme was employed to discretize the ordinary differential equation system, simplifying the solution process. For Problem 2, building on Problem 1, an optimization model for maximum power output was established, considering the periodic nature of the motion. A binary search was initially used to find the optimal solution for one period, which reduced the model complexity. Because of the non-monotonic nature of average output power with respect to

damping coefficients, the binary search may not yield the optimal solution. Further optimization was carried out by the steepest descent method, but efficiency was found to be suboptimal. Finally, the Matlab fminsearch function was employed to simplify model calculations.

For Problem 3, the model from Problem 1 was extended to consider the gravitational force on the pendulum, introducing an angle between the direction of gravity and the pendulum's oscillation. Further force analysis was conducted to establish a mathematical model, which reduced the model complexity. The equations of motion for pitch and buoy oscillation were obtained through force and torque analyses. The Euler-predictor-corrector scheme was again used for model solution, ensuring simplicity and feasibility. For Problem 4, an optimization model for the damping coefficients of the linear damper and rotational damper was established on the basis of that of Problem 2, enhancing model reliability. Smart algorithms were employed to simplify model calculations. Sensitivity analysis showed good stability, affirming the reliability of the model. Additionally, tMFPA was used to validate the results, and the model's reliability was confirmed. On the basis of the results of the mechanical analysis of wave energy devices, we obtained a motion model for the device transitioning from one dimension to two dimensions. Through the analysis of the motion model, we conducted an analysis of the maximum average output power of wave energy, providing insights for the analysis of the device's motion in more dimensions. This work yielded valuable insights into the research direction of power optimization control for wave energy generation devices. It can serve as a reference for further research and exploration in the field of wave energy, especially in understanding and optimizing the power output of devices operating in multiple dimensions.

Acknowledgments

This research was supported through projects under grant No. CS−111−03, by Summit-Tech Resource Corp. and by Nos. MOST 111−2221−E−390−018 and NSTC 112−2622−E−390−002.

References

1 N. Ding, J. Yang, H. Cheng, and Q. Dai: IOP Conf. Ser.: Earth Environ. Sci. **651** (2021) 022088.
2 K. Veerabhadrappa, B. G. Suhas, C. K. Mangrulkar, R. Suresh Kumar, V. S. Mudakappanavar, Narahari, and K. N. Seetharamu: Global Transitions Proc. **3** (2022) 359.
3 J. Yan, N. Mei, D. P. Zhang, Y. Zhong, and C. Wang: Front. Energy Res. **19** (2022) 966567.
4 T. K. A. Brekken, B. Batten, and E. A. Amon: IEEE Control Syst. **31** (2011) 18.
5 N. A. Mohd Fadzil, A. M. Ishak, A. S. Abu Hasim, S. M. F. Syed Mohd Dardin, and A. Abdul Azid: 2018 Int. Conf. Electrical Engineering and Computer Science (ICECOS), Pangkal, Indonesia (2018) 287.
6 P. Beirão and C. Malça: Int. J. Energy Environ. Eng. **5** (2014) 1.
7 R. Song, M. Zhang, X. Qian, X. Wang, M. Dai, and J. Chen: J. Mar. Sci. Eng. **4** (2016) 35.
8 A. Azam, A. Ahmed, H. Li, A. M. Tairab, C. Jia, and N. Li: Ocean Eng. **255** (2022) 111434.
9 W. Lai, D. Li, and Y. Xie: Ocean Eng. **232** (2021) 109080.
10 A. Ahmed, A. Azam, Y. Wang, X. Tan, M. Yi, and Z. Zhang: Energy Convers. Manage.: X **19** (2023) 100387.
11 S. Chiba, M. Waki, C. Jiang, M. Takeshita, M. Uejima, K. Arakawa, and K. Ohyama: Energies **14** (2021) 3414.
12 F. Mwasilu and J. W. Jung: IET Renewable Power Gener. **13** (2019) 363.
13 V. M. Solanki: Int. J. Eng. Res. Technol. **10** (2021) 91.
14 M. S. Amin: Electr. Electron. Eng. (2023). https://doi.org/10.20944/preprints202306.0277.v1
15 E. García, E. Quiles, A. Correcher, and F. Morant: Sensors **18** (2018) 945.
16 X. Liu, Z. Chen, and M. Li: China Automation Congress (CAC), Beijing, China (2021) 7801.

17 G. Reikard: Ocean Eng. **73** (2013) 168.
18 A. H. Workie: Abstr. Appl. Anal. **2021** (2021) 9951815.
19 Y. Bella and K. F. Zohra: Eng. Technol. Appl. Sci. Res. **12** (2022) 8548.
20 L. F. Lee and B. R. Umberger: PeerJ **4** (2016) e1638.
21 J. Wu, N. Chen, and C. Qian: J. Mech. Eng. **58** (2022) 222. (in Chinese)
22 F. M. Creevey, C. D. Hill, and L. C. L. Hollenberg: Sci. Rep. **13** (2023) 11956.
23 K. M. Ong, P. Ong, and C. K. Sia: Decis. Anal. J. **5** (2022) 100144.